Heliyon 10 (2024) e25425

Contents lists available at ScienceDirect

Heliyon

journal homepage: www.cell.com/heliyon

Research article

Preparation and characterization of pristine and Sn doped copper gallium sulphide (CGS) thin films using spray pyrolysis technique

Sreelakshmi Krishna *, V. Vasu

School of Physics, Madurai Kamaraj University, Madurai, Tamil Nadu, India

ARTICLE INFO

Keywords:
Spray pyrolysis
Thin films
Sn doped CGS
$CuGaS_2$ films
Chalcopyrite
Solar cells

ABSTRACT

With thin film solar cell applications, chalcopyrite semiconductors present enormous potential for usage as an absorber layer. In today's electronics sector, wide band gap semiconductors have extreme demand for applications such as high-power, high-frequency, challenging devices that are resistant to high temperatures, optoelectronic devices, and short-wavelength light-emitting devices. The undoped and tin-doped CGS thin films are the subject of the current investigation. Pure and Tin (Sn) doped CGS thin films were produced on a glass substrate using a low-cost chemical spray pyrolysis technique in a nitrogen atmosphere. Spray pyrolysis is a flexible and efficient method for thin-film deposition. The process parameters, such as the nozzle distance, spray time, spray rate, and temperature, have a significant impact on the films' quality and characteristics. Fundamental characterization techniques, including XRD analysis, Micro Raman analysis, EDAX, UV-VIS-NIR spectroscopy, and Scanning Electron Microscopy (SEM), were used to examine the generated pristine and Sn-doped CGS thin films. The XRD patterns showed that the pristine and Sn-doped CGS thin films exhibit a tetragonal phase and there is a decrease in the crystallite size with increasing dopant concentration. SEM studies revealed that there is a change in the grain size and surface morphology of the film with increasing Sn doping concentration. The presence of copper (Cu), gallium (Ga), sulfur (S), and Sn was further confirmed by studying the EDAX spectrum. SEM results indicate that the surface morphology of the CGS films is modified by Sn doping. Further increasing the dopant percentage caused deformation and fragmentation of the sample. A comparison of the Raman spectra for pristine and Sn-doped CGS revealed that there is some substantial change in the layer composition after adding the dopant. Compared to the pristine CGS, the peak positions of CGS (1 wt %) and CGS (3 wt %) are not shifted but there is a significant change in the relative peak intensities and formation of an additional peak The Sn-doped $CuGaS_2$ thin films had optical band gaps of 2.47 eV (0.0 wt% Sn-doped), 2.33 eV (1 wt % Sn-doped), and 2.58 eV (3 wt% Sn-doped). From this study, we can say that the 1 wt% Sn doped CGS sample is the best for solar cell application. The XRD results indicated that the Sn dopant addition in the $CuGaS_2$ lattice site does not affect the symmetry of the material. Enhancement of absorption is done by the Sn dopant.

1. Introduction

One of the most significant issues affecting humanity is the energy crisis, which is caused by an inadequate supply of power and

* Corresponding author.
E-mail addresses: sreelakshmi.krishna48@gmail.com (S. Krishna), vasu.physics@mkuniversity.ac.in (V. Vasu).

https://doi.org/10.1016/j.heliyon.2024.e25425
Received 7 October 2023; Received in revised form 12 January 2024; Accepted 26 January 2024
Available online 28 January 2024

ongoing population expansion. Solar energy is among the most reliable and renewable means of meeting the energy demands of modern era, more so than geothermal, hydropower, wind energy etc. The annual solar energy reaching the planet's surface surpasses the whole quantity of commercial energy used by mankind today. Due to the abundant and inexhaustible solar energy, extensive research into solar cells has recently been conducted. The most attention has been focused on silicon-based solar cells because of their excellent conversion efficiency [1]. However, because of the indirect bandgap, Si has a low absorption coefficient. Therefore, for the material to effectively absorb solar energy, a thick layer of it is required. Another disadvantage of Si-based solar cells is their use of expensive, dangerous chemicals [2]. The creation of solar cells with high conversion efficiency from inexpensive, direct bandgap materials has drawn more attention in recent years. Given that photons with specific wavelengths are exclusively utilized to move electrons from the valence band to the conduction band, further advancements in conversion efficiency will be essentially constrained. The rate of electron-hole pair recombination and absorbance in the light spectrum region are the main factors influencing the conversion efficiency of solar cells. By modifying the characteristics of the absorber layers used in solar cells, it is possible to enhance the absorption region in the solar spectrum and obtain high conversion efficiency. Cu (In_{1-x} Ga_x)Se_2 (CIGS), a semiconductor made of chalcopyrite, is a popular material for solar cell fabrication because of its excellent radiation stability, high absorption coefficient (=105 cm −1), and other characteristics [3]. The manufacturing cost of the solar cell, which is prohibitively high while having a conversion efficiency of up to 20.3 % [4], is related to the In element's rarity and high cost. Sol-gel method [5,6], electrodeposition [7], ink coating [8], ball milling [9], paste coating [3], chemical bath deposition [10], and other processes have all been developed for the synthesis of CIGS. However, these techniques still have some flaws, including costly vacuum technology, chemical pollution, etc. In this paper, the fabrication and experimental validation of Sn-doped $CuGaS_2$ thin films, a chalcopyrite semiconductor material, using spray pyrolysis is reported. In the past, Ti-doped CuGaS2 [11], Mn-doped CuGaS2 [12], and Cr-doped CuGaS2 [13,14] intermediate band materials have also shown partial dopant replacement for Ga. The use of this method to deposit CuGaSnS2 thin films for solar cell applications has been documented in a very small number of studies. The optical, morphological, and structural properties of CGS films are compared to those of pure CGS to study the effects of Sn doping. Since we may choose the proportion of the precursor solution to form a variety of compounds, this method makes it easier to control the element components. By substituting In for Sn, it is possible to further modify the thin films, which makes it cost effective. Additionally, the surface morphology, the structure of $CuGaS_2$ thin films that have been doped with Sn, and the effect of Sn doping at various concentrations on the band gap were investigated utilizing a range of characterization techniques. Spray pyrolysis offers a lot of potential for use in making inexpensive thin-film solar cells. Chalcopyrite $CuGaS_2$ solar cells are already commercially accessible, however by employing inexpensive techniques like spray pyrolysis, they can be made more affordable [15–21].

In the current work, a general model for spray pyrolysis is being proposed. This work is based on numerous experimental investigations that have produced both general and comprehensive observations. In this study, spray pyrolysis was used to create thin films of $CuGaS_2$ that were Sn-doped. Further investigations have been done on their characterization using techniques including XRD analysis, Raman analysis, surface morphology (SEM and EDAX), structure, and UV–Vis analysis of Sn-doped $CuGaS_2$ thin films. It has also been addressed how Sn concentration affects band gap.

2. Materials and methods

2.1. Material introduction

A semiconductor with a direct band gap in the range of 2.47 eV, $CuGaS_2$ (CGS) is a ternary chalcopyrite compound with the general formula $CuME_2$ (M = Ga; E = S). It is useful for solar applications [22–24]. One of the most significant semiconductor materials that can be used to create inexpensive photovoltaic devices is chalcopyrite Cu (In, Ga) Se2 (CIGS) [25]. $CuGaS_2$ has been considered as a promising material having the potential for next-generation solar cells. $CuGaS_2$ thin-film solar cells have been shown to produce efficiencies above 20 % in laboratory conditions, making such types of materials highly desirable for application in large-area solar modules. Numerous investigations have been conducted to investigate the physical and chemical properties of ternary chalcopyrite since the first report of its synthesis and structural characterization. $CuGaS_2$ is one of the materials in this family; nevertheless, it is not

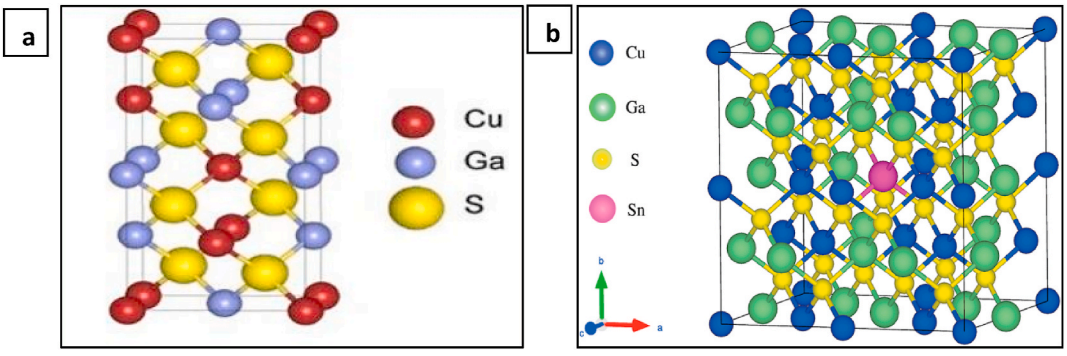

Fig. 1. (a). Tetragonal crystal structure of $CuGaS_2$ and (b) Sn doped $CuGaS_2$.

suitable as a light-absorbing layer for single junction solar cell applications because of its greater direct band gap, which is about 2.47 eV at ambient temperature [26]. Additionally, CuGaS2 has been considered as a promising candidate for use in devices that emit visible light. Direct band gap semiconductors are preferable to indirect band gap crystalline silicon in several ways. Because of their lower absorption coefficients, indirect band gap semiconductors need extensive absorber layers to absorb sufficient light, which could lead to undesirable results. They possess a notable optical absorption coefficient (10^5 cm^{-1}) and provide the highest conversion efficiencies among thin-film methods at the laboratory scale [27]. CGS is a p-type semi-conductor, and it possesses a tetragonal crystal structure. I-III-VI_2 tetragonal chalcopyrite crystals of $CuGaS_2$ form the tetragonal crystal structure of $CuGaS_2$ as shown in Fig. 1 (a) and Sn doped $CuGaS_2$ as shown in Fig. 1 (b).

Shay and Wernick provide an overview of several of its properties in their study [28]. Doping techniques can modify this material's conductivity. CGS can therefore function as p-type and n-type semiconductors. Therefore CGS is a promising host material for several applications [29]. Processes such as solution growth, chemical vapor deposition, electron beam evaporation technique, have been used to deposit $CuGaS_2$ thin films [30,31]. Chemical spray pyrolysis is thought to be the most effective and simple approach for synthesizing thin films. Scalability, affordability, ease of doping, ease of operation at moderate temperatures, which allows for a wide range of substrates, ability to control thickness, ability to modify film composition, and the capacity to deposit multiple layers are the main advantages of this method over other deposition processes.

2.2. Experimental details

Microscopic glass slides of size 7.5 cm × 2.2 cm x 0.125 cm are the substrate used. Before deposition, the substrate is ultrasonically cleaned using distilled water, acetone, and chromic acid. To make the $CuGaS_2$ precursor solution, 0.1 mol of Copper Chloride, 0.1 mol of Gallium nitrate, and 0.3 mol of Thiourea were added to 45 ml of double distilled water (DDW) [32]. Sulfur evaporates quickly; therefore, the sample would lack sulfate content as a result. To avoid this excess, thiourea was added to make up for the sulfur lost during the pyrolysis process. Tin chloride was employed as the Sn ion source substance for doping. $SnCl_3$ was added into the pristine CGS precursor solution at various weight percentages. After 30 min of thorough stirring, the final precursor solution—which was clear and homogenous—was prepared. The pre-heated glass substrate was sprayed with the precursor solution. To deposit both pristine CGS and CGS films doped with Sn, the substrate temperature was held constant at 200 °C.

Fig. 2(a) and (b) illustrate the prepared films (pristine and Sn doped CGS), respectively. For every deposition, the nozzle-to-substrate distance was maintained at 28 cm. The carrier gas pressure (compressed air −40 kg/cm^2), spray time (3 s), and spray rate (3 ml/min) were all adjusted to yield high-quality films. Following the deposition, the coated substrates were allowed to cool to room temperature. Annealing was carried out at 350 °C in a tube furnace in a N_2 atmosphere.

2.3. Characterization

The $CuGaSnS_2$ thin films' crystallographic characteristics were determined through the examination of X-ray radiation patterns produced by a Bruker D8 Discover diffractometer and intense CuKα radiation (λ = 1.5405 Å). The thin film was subjected to Raman examination using a Renishaw QONTOR Raman Spectrometer. The employed laser had a 532 nm wavelength and a 5 % power output, or 2.5 mW. There were ten acquisitions made in 1 s of acquisition time. At room temperature, samples were scanned within the range of 100–700 cm^{-1}. The Carl Zeiss Merlin VP Compact FESEM was connected to a Bruker XFlash 6130 EDX Spectrometer, which was used to take the sample's EDX. The Carl Zeiss Merlin VP Compact Scanning Electron Microscope was used to get the SEM pictures. Using a UV–Vis spectrophotometer of model UV-2600,SHIMADZU, the optical absorption spectra of pristine CGS and Sn doped CGS films were recorded in the range of 200–1400 nm wavelength (Fig. 8).

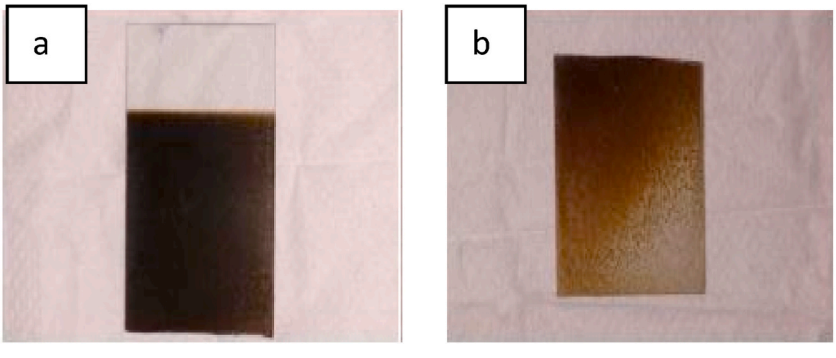

Fig. 2. (a) Pure and (b) Sn doped CGS thin films deposited on glass substrates.

3. Results and discussions

3.1. X-ray diffraction analysis

The XRD measurement is done using Copper Kα X-Ray source. Structural studies were carried out. The peaks present in our sample are compared with the powder diffraction files (PDF) database to identify the material. The peak position gives information about the material. For example the inter planar spacing 'd' for a cubic crystal can be obtained from Bragg's law (Equation 1) and the lattice constant 'a' can be obtained from Equation 2. The miller indices and diffraction angle for the calculation can be obtained from the diffractogram [33].

$$n\lambda = 2d \sin \Theta \quad [1]$$

$$a = d\sqrt{h^2 + l^2 + k^2} \quad [2]$$

As a function of different Sn concentrations (1 wt% & 3 wt%) in the precursor solution, the XRD pattern of pure CGS and Sn doped CGS thin films formed by spray pyrolysis technique is shown in Fig. 3, revealing the polycrystalline nature of the films.

When compared to JCPDS file No.00-025-0279, the presence of peaks in the XRD patterns indicates that all the samples correspond to the tetragonal chalcopyrite phase with a dominating peak at (112) [34]. The XRD patterns of the sample showed strong (112) preferred orientation peaks that were intense, indicating high crystallinity [3]. Significantly, the FWHM of the (112) diffraction peak has decreased with the addition of 1 wt % of Sn. The films showed a growth orientation along (112), (220) and (204) planes. It was found that the FWHM of the (112) plane increased to a lower value as the Sn concentration was increased to 3 wt %.

For all samples, the position of the most intense peak (112) was compared in Fig. 3(b). It is discovered that the (112) peak position of Sn doped CGS thin films tends to shift toward higher 2θ angles after Sn-doping. At 28.86°, 28.91°, and 28.99°, respectively, the predominant peaks of the Sn doped $CuGaS_2$ thin films with different Sn concentrations of 0 wt%, 1 wt%, and 3 wt% can be seen. This shift in the FWHM indicates that Sn has been incorporated into the chalcopyrite lattice, changing the interplanar distance [35]. The difference between the atomic radii of Ga (1.26 Å) and Sn (1.40 Å) may have led to the substitution of Sn ions into the Cu or Ga lattices or the occupation of an interstitial site. As Ga always tends to evaporate and comparatively has low cohesive energy, it increases the probability of Ga to get replaced by Sn. Table 1 presents the calculated values of the lattice constants. Changes in the lattice properties result from doping Sn into the host $CuGaS_2$, and these variations are dependent on the doping concentration [36]. For pure 1 wt percent and 3 wt percent, the unit cell parameter "a" It was discovered that Sn doped CGS was 5.34 Å, 5.32 Å, and 5.33 Å, in sequence. Shrinkage of the lattice parameter (a = 5.34 Å→5.32 Å) might also have been a reason for the decrease in the FWHM of the peak on adding 1 wt % of Sn dopant [37]. When interatomic spacing decreases, larger Sn^{4+} ions (1.40 Å atomic radius) are replaced by smaller Ga^{3+} ions (1.26 Å atomic radius), which has resulted in a slight decrease in lattice constant [38]. On further increasing the Sn concentration by 3 wt % there is a decrease in the peak intensity which is due to the complete replacement of either the Ga or Cu lattice sites by excess of Sn^{4+} or by the occupation of Sn into interstitial sites of CGS thereby dominating the properties of CGS material which changes or suppresses the properties of the CGS material.

The lattice parameters of the crystallographic systems in the current study are calculated using the relation, given in Equation (3), with (h k l) parameters and interplanar spacing, "d," where h, k, and l are the plane's Miller indices.

$$\frac{4\,sin^2\theta}{\lambda^2} = \frac{1}{d^2} = \frac{h^2 + k^2}{a^2} + \frac{I^2}{C^2} \quad [3]$$

The (112) and (220) peaks served as the basis for the calculation of the lattice parameters displayed in Table 1. The lattice

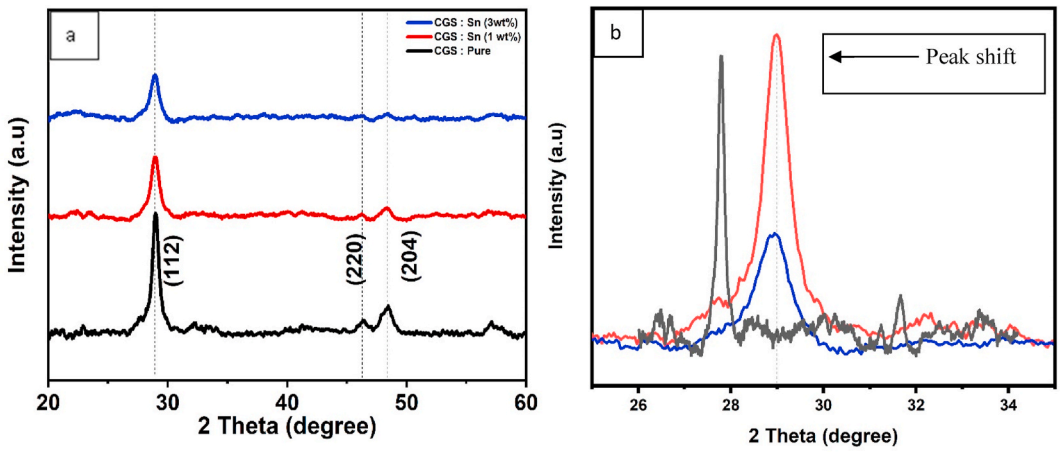

Fig. 3. (a) XRD pattern of pristine and Sn doped $CuGaS_2$ thin films (b) observed peak shift.

Table 1
X-ray diffraction data for pristine and Sn doped CGS thin films.

Sample	Plane (hkl)	d spacing (Å)	2Θ	Θ	FWHM (β)	Lattice parameter (Å)	Anion displacement	Crystallite size (D in nm)
$CuGaS_2$ (pristine)	(112)	3.09	28.97	14.43	0.0196	a = 5.34 c = 10.78	0.244	7.30
$CuGaS_2$ (Sn 1 wt%)	(112)	3.07	28.89	14.49	0.0130	a = 5.32 c = 10.69	0.247	11.01
$CuGaS_2$ (Sn-3 wt. %)	(112)	3.08	28.97	14.45	0.0173	a = 5.33 c = 10.76	0.244	8.27

parameter values that were obtained for pure, 1 wt percent, and 3 wt percent, respectively, are a = 5.34 Å, 5.32 Å, 5.33 Å, and c = 10.78 Å, 10.69 Å, and 10.76 Å, showing a strong correlation with the data reported in the literature [39]. The Scherrer formula, found in Equation (4), was used to determine the average crystallite size of the films. The formula considers the following values: λ (=1.5406 Å), the X-ray source's wavelength, β (the FWHM value in radians), and Θ is the Bragg's angle or diffraction angle. This formula is somewhat arbitrary and falls between 0.87 and 1.0. Table 1 and Fig. 4 demonstrate the variation of crystalline size as a function of Sn concentration.

$$D = \frac{K\lambda}{\beta \cos \Theta} \quad [4]$$

The crystallite size of CGS film increases on adding 1 wt % of the Sn dopant. But on further increasing the dopant concentration to 3 wt % there is a decrease in the crystallite size. This may be due to the smaller ionic radius of Ga^{3+} ions (0.62 Å) than that of Sn^{4+} ions (0.69 Å) [40]. The maximum crystallite size of 11 nm is found for 1 wt % of Sn doped CGS film and a minimum of 7 nm is found for pure CGS film [41,42]. It can be seen that on adding the Sn dopant, the particles or grains on the film surface are clustered together to form a densely packed structure but on further increasing the dopant concentration to 3 wt %, deformation of the material occurs and the material loses its crystalline nature due to which fragmentation of the grains into smaller particles or grains occur which in turn becomes the reason for a decrease in the crystallite size, on increasing the dopant concentration.

Correlations exist between the results and the XRD spectra. The anion displacement of CuGaSnS2 thin films was calculated using the relation provided in Equations (5a) and (5b), where "w" is the anion displacement and "a" and "c" are the lattice parameters. Table 1 lists the determined anion displacement values. The anion displacement values of all the samples showed no significant change, suggesting that the Sn dopant addition in the $CuGaS_2$ lattice site has no effect on the symmetry of the material.

$$w = \frac{1}{2} - \left[\frac{C^2}{32a^2} - \frac{1}{16}\right]^{1/2} \quad [5\ a]$$

$$\text{i.e. } \frac{c2}{a2} = 2 + 32(0.5 - w) \quad [5\ b]$$

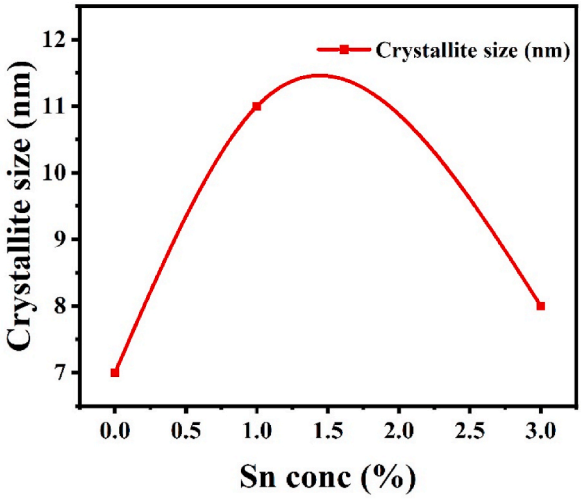

Fig. 4. Variation of crystallite size with respect to Sn dopant wt %.

3.2. Micro Raman analysis

The Raman active modes for pure CGS, Sn doped CGS (1 wt%), and Sn doped CGS (3 wt%) were examined at room temperature to understand the impact of Sn doping on the structure. The micro-Raman spectrum of pure and Sn-doped CGS (1 wt% Sn and 3 wt% Sn) thin films is shown in Fig. 5.

Three prominent peaks can be observed in the CGS sample at around 306 cm^{-1}, 382 cm^{-1}, and 469 cm^{-1} [43]. The most significant active mode in the chalcopyrite spectra of CuGaS2 is the A1 phase of CGS, which is responsible for the strong modes observed at 306 cm^{-1} [44]. The A1 mode is exclusively anionic. This mode is the symmetric vibration of sulfur atoms in which the S atom is moving and the other atoms in the lattice, the Cu and Ga atoms, are at rest [45,46]. Additionally, the S–S stretching mode of S_2 ions is represented by the mode corresponding to 469cm-1 [47,48]. The low intense mode at 382 cm^{-1} is related to the B_2 LO (Longitudinal Optical) mode which is attributed to the high frequency band vibrations of Ga–S bond [49,50]. The CGS (1 wt percent) and CGS (3 wt percent) peak positions are not altered in relation to the pure CGS peak, but there is a notable shift in the relative peak intensities, and an extra peak is seen to develop at 339 cm^{-1}. As can be seen in Fig. 5, adding 1 wt percent of the Sn dopant causes a little decrease in the peak's intensity at 306 cm^{-1}. The peak intensity decreases, and an additional peak appears upon increasing the dopant concentration to 3 wt percent. The Sn–S_2 bond's vibration is what caused this extra peak to develop. With eight atoms per unit cell, the CGS crystallizes in the chalcopyrite structure [51]. The information presented above showed that the crystal structure is significantly influenced by the bonding conditions.

3.3. EDS analysis

The elemental concentration of pristine and Sn doped CuGaS2 thin films with representative EDAX [52] spectra at varying Sn concentrations of (a) 0.0 wt% of Sn, (b) 1.0 wt% of Sn, and (c) 3.0 wt% of Sn are shown in Fig. 6 (a), (b) and (c). Consequently, the EDAX spectrum revealed that the elements Cu, Ga, S, and Sn was present in the sample with their relative amounts as given in Table 2. The concentrations of the films of Cu, Ga, S, and Sn match that of the preparation solution.

3.4. Scanning Electron Microscopy (SEM)

Surface morphological (SEM) images of pure CGS and Sn-doped CGS thin films at Sn concentrations of 1 wt % and 3 wt % are given in Fig. 7 (a), (b) and (c) respectively. The differences in grain size and morphology as a result of sample doping are depicted in the plane-view SEM images in Fig. 7 (a), (b) and (c) respectively. The grains or granules that form on the surface of pure CGS film are seen to have an abundance of irregular sizes, shapes, and separations. The CGS films demonstrated a compact adherence to the glass substrate with no cracks or voids, despite not being tightly packed. For pure CGS thin films, the grains are loosely packed; however, as the concentration of Sn increases, the grains become firmly packed and exhibit noticeable alterations in size. Sponge-like structures are closely packed on the surface at a doping concentration of 1 wt percent.

The SEM image demonstrates that there are no pinholes [53] and that the surface is completely covered in grains [7]. Thus, we can say that with increase in the Sn concentration to 1 wt % the sample became more uniform and denser. On further increasing the Sn doping level to 3 wt % material deformation occurs and the material loses its crystalline nature due to which fragmentation of the densely packed grains into smaller particles occur which in turn becomes the reason for a decrease in the crystallite size, on increasing the dopant concentration. As a result, the grains are not evenly dispersed throughout the surface, and droplet-like formations with approximately uniform sizes are present. Sn doping alters the surface morphology of the CGS films. Therefore, we can conclude that the various concentrations of Sn doping in the precursor solution effectively alter the surface morphology of the CGS films, and the outcomes may correlated to the XRD data.

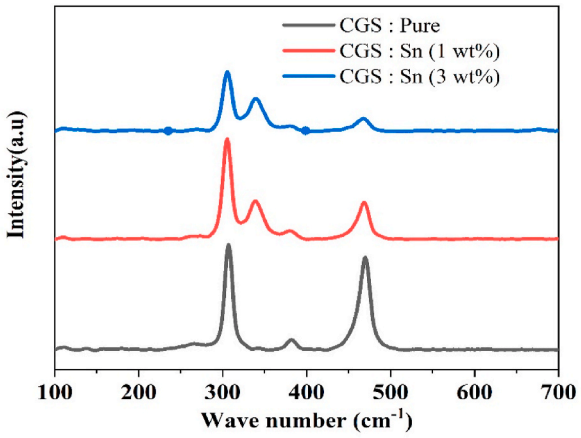

Fig. 5. Micro Raman Spectrum of pristine and Sn doped CGS thin films.

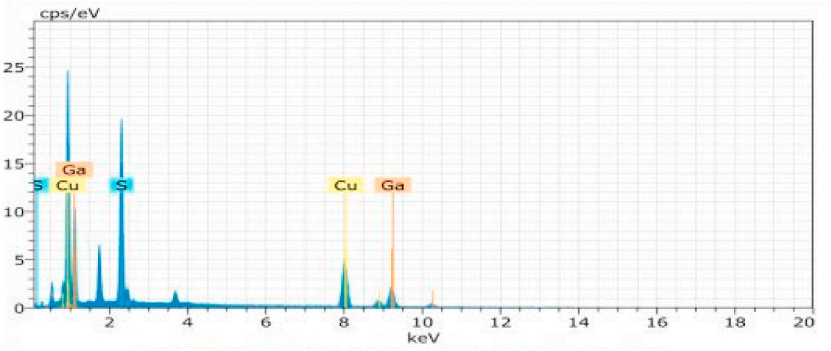

(a) EDAX spectrum of pure CGS thin film

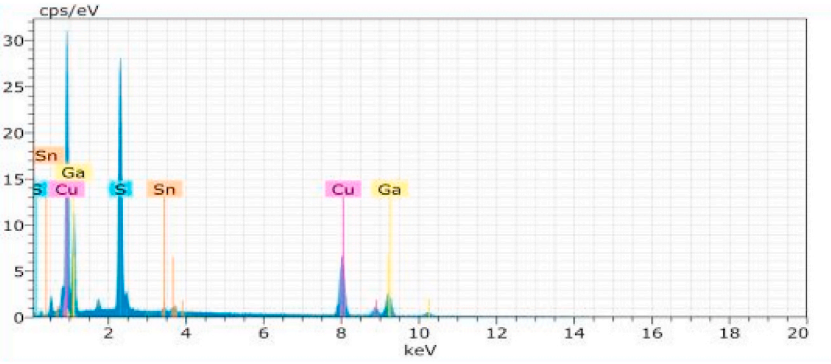

(b) EDAX spectrum of 1 wt.% Sn doped CGS thin film

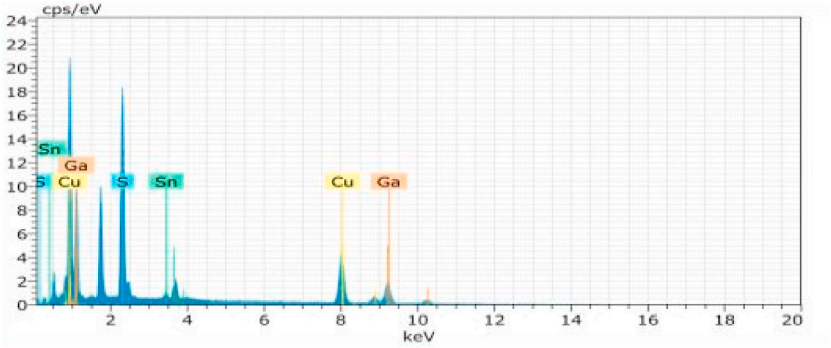

(c) EDAX spectrum of 3 wt. % Sn doped CGS thin film

Fig. 6. (a) EDAX spectrum of pure CGS thin film. (b) EDAX spectrum of 1 wt% Sn doped CGS thin film. (c) EDAX spectrum of 3 wt % Sn doped CGS thin film.

Table 2
Representation of atomic weight % of undoped and Sn doped CGS thin films.

Elements	Pure CGS	1 wt% Sn doped CGS	3 wt% Sn doped CGS
S	42.04	44.10	42.43
Cu	33.75	34.55	32.94
Ga	24.21	20.64	22.10
Sn	0	0.71	2.54

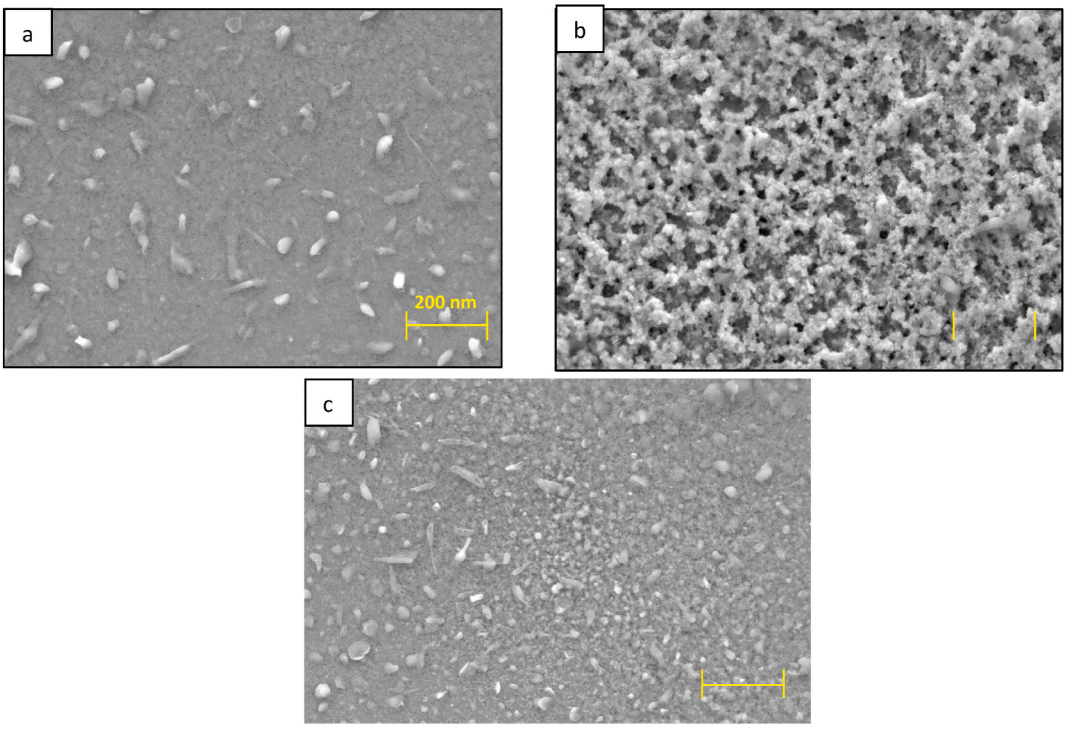

Fig. 7. SEM images of the CGS thin films deposited on glass substrate as a function of varying dopant concentration (a) pure, b) 1 wt %, c) 3 wt% respectively).

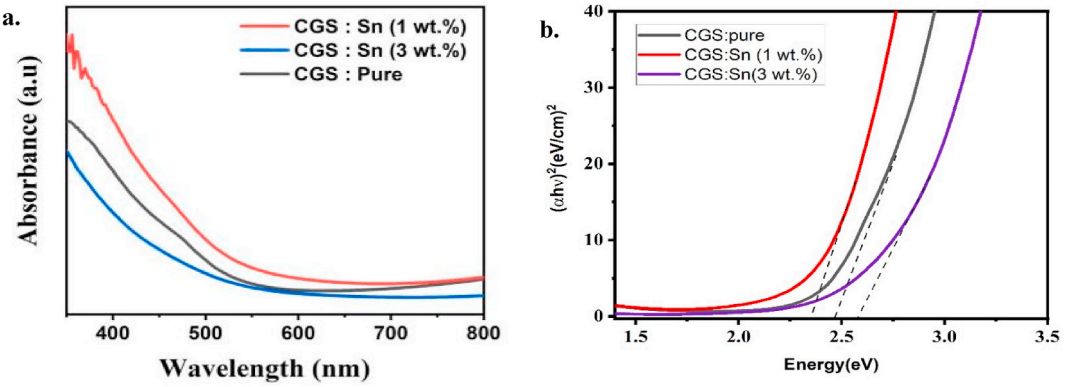

Fig. 8. (a). Optical absorption spectrum of pristine and Sn doped CGS thin films (b). Optical band gap of pristine and Sn doped CGS thin films.

3.5. UV-VIS-NIR analysis

The photon energy (hν) and the absorption coefficient (α) for a permitted direct band gap transition can be connected using the Tauc's relation, as shown in Equation (6) [54], where hν is the incident photon energy (h-Planck's constant & ν-frequency), A is the constant, and α is the absorption coefficient.

Fig. 8(a) shows how the absorption coefficient varies with wavelength. The direct band gap, also known as the optical band gap, is found by extending the linear regression curve that emerges from a plot of photon energy (hν) vs ($\alpha^*\nu$)2 to the hν axis (Fig. 8(b)) [55].

$$\alpha = A\ (h\nu - Eg)^{1/2} \quad [6]$$

The linear relationship found in Fig. 8 (b) implies that all $CuGaS_2$ thin films exhibited a direct band gap [56]. Table 3 provides the band gap values that were computed. The direct band gap (2.47 → 2.33eV) decreases first when the weight percentage of Sn is raised to 1 wt percent, according to the optical band gaps for the three compounds. The reason for this drop in the band gap value is due to the tendency of Sn ions to substitute and replace the Cu or Ga ions from their lattice sites. However, as the wt. % of the Sn dopant is

Table 3
Band gap values of pure and Sn doped CGS thin films.

Sample	Band gap (eV)
$CuGaS_2$ (pure)	2.47
$CuGaSnS_2$ (Sn-1 wt.%)	2.33
$CuGaSnS_2$ (Sn-3 wt.%)	2.58

increased to 3 wt % an increase in the direct band gap (2.47 → 2.58eV) is observed which is due to the complete replacement of either Cu or Ga^{2+} from its lattice sites by excess of Sn4+ ions or by occupation of Sn^{4+} in the interstitial sites of CGS. This indicates that on increasing the dopant concentration the material loses its crystalline nature, deforms, forms small fragments, and loses its identity hence showing a band gap higher than that of the band gap of the CGS material. The decreasing grain size causes an increase in the bandgap, which can be due to Burstein-Moss shift/effect (B-M effect). The ability to generate different optical properties for the same material makes the B-M effect significant. It suggests that the optical band gap of degenerately doped semiconductors increases when all states near the conduction band get populated due to shifting of an absorption edge to higher energy [57].

Wide band gap materials have several applications. The compound $CuGaS_2$ has a measured direct band gap of 2.46 eV. The change in band gap values while increasing the doping level can be related with the data published in literature [58].

4. Conclusions

The $CuGaS_2$ thin films with a tetragonal polycrystalline structure were created on glass substrates using the spray pyrolysis process. The low-cost spray pyrolysis method was effectively used to deposit the pristine and Sn-doped CGS thin films. From XRD and Raman Spectra it was concluded that the pristine and Sn doped CGS possess the tetragonal phase. Apart from this, from the Raman spectra it was observed that there was no peak shift, but the intensities of the peaks reduced on increasing dopant concentration as well as additional peaks were observed. The presence of Cu, Ga, S and Sn were confirmed using EDAX analysis. The surface morphology of pristine and Sn doped CGS were characterized by SEM analysis. From the images, we can conclude that the particles have irregular grain like structure. From the absorption spectra of pristine and Sn doped CGS, the optical band gap values were calculated. The sample showed a direct band gap energy in the range of Eg = 2.47 eV for CGS pure and for 1 wt% of Sn, Eg = 2.33 eV and for 3 wt% of Sn, Eg = 2.58 eV which is a wide band gap and has several applications. From this study we can say that the 1 wt% Sn doped CGS sample is the best for solar cell application. The results indicate that Sn doped CGS is a promising material for several applications.

Data availability

No external data was used for the research described in the article.

CRediT authorship contribution statement

Sreelakshmi Krishna: Writing – original draft, Methodology. **V. Vasu:** Writing – review & editing, Supervision.

Declaration of competing interest

The authors declare the following financial interests/personal relationships which may be considered as potential competing interests:Sreelakshmi Krishna reports writing assistance was provided by Madurai Kamaraj University School of Physics. Sreelakshmi Krishna reports equipment, drugs, and supplies were provided by Madurai Kamaraj University School of Physics. The author and co-author have been previously employed with this organization. The former has completed the respective course, and the latter has completed his period of service from the same organization. This work has been submitted after these events. If there are other authors, they declare that they have no known competing financial interests or personal relationships that could have appeared to influence the work reported in this paper.

Acknowledgments

The author Sreelakshmi Krishna gratefully acknowledge Dr K Sethuraman (Associate Professor, Central University of Tamil Nadu), Hari Ramprasath (Research Scholar, Central University of Tamil Nadu) and Dr S Suba Viveka (Assistant Professor, NMS.S.V.N College) for providing all the support throughout this work.

References

[1] N.E.B. Cowern, Silicon-based photovoltaic solar cells, Funct. Mater. Sustain. Energy Appl. (2012), https://doi.org/10.1533/9780857096371.1.1, 3–22e.
[2] Z. Zongyan, Z. Dacheng, Y. Juan, Analysis of the electronic structures of 3d transition metals doped CuGaS2 based on DFT calculations, J. Semiconduct. 35 (2014) 13002, https://doi.org/10.1088/1674-4926/35/1/013002.
[3] S. Song, Y. Wang, X. Yuan, W. Yao, W. Jing, Characterization and preparation of Sn-doped $CuGaS_2$ thin films by paste coating, Mater. Lett. 148 (2015) 41–44, https://doi.org/10.1016/j.matlet.2015.02.041.

[4] T. Ibn-Mohammed, S.C.L. Koh, I.M. Reaney, A. Acquaye, G. Schileo, K.B. Mustapha, R. Greenough, Perovskite solar cells: an integrated hybrid lifecycle assessment and review in comparison with other photovoltaic technologies, Renew. Sustain. Energy Rev. 80 (2017) 1321–1344, https://doi.org/10.1016/j.rser.2017.05.095.

[5] Gaurav Bahuguna, Neeraj Kumar Mishra, Pratibha Chaudhary, Kumar Amit, Rajeev Singh, Thin film coating through sol-gel technique, Res. J. Chem. Sci. 6 (7) (2016) 65–72.

[6] U.C. Matur, N. Baydogan, Sol–gel derived Cu(in,Ga)Se $_2$ thin film solar cell, J. Nanoelectron. Optoelectron. 12 (4) (2017) 352–358, https://doi.org/10.1166/jno.2017.2023.

[7] Z. Cao, S. Yang, M. Wang, X. Huang, H. Li, J. Yi, J. Zhong, Electrodeposition of Cu–Ga precursor layer for $CuGaS_2$ solar energy thin film from alcohol solution, Ionics 23 (4) (2017) 1027–1033, https://doi.org/10.1007/s11581-016-1888-6.

[8] M. Kemell, M. Ritala, M. Leskelä, Thin film deposition methods for CuInSe 2 solar cells, Crit. Rev. Solid State Mater. Sci. 30 (1) (2005) 1–31, https://doi.org/10.1080/10408430590918341.

[9] X. Zhang, Q. Sun, M. Zheng, Z. Duan, Y. Wang, Solar cell applications of solution-processed AgInGaSe2 thin films and improved properties by sodium doping, Nanomaterials 10 (3) (2020) 547, https://doi.org/10.3390/nano10030547.

[10] Luidmila L. Larina, Kihwan Kim, Kyung Hoon Yoon, M. Konagai, Thin film CIGS-based solar cells with an In-based buffer layer fabricated by chemical bath deposition, in: Photovoltaic Energy Conversion, 2003. Proceedings of 3rd World Conference, 2003.

[11] X. Lv, S. Yang, M. Li, H. Li, J. Yi, M. Wang, G. Niu, J. Zhong, Investigation of a novel intermediate band photovoltaic material with wide spectrum solar absorption based on Ti-substituted CuGaS2, Sol. Energy 103 (2014) 480–487, https://doi.org/10.1016/j.solener.2014.02.046.

[12] P. Prabukanthan, R. Dhanasekaran, Influence of Mn doping on CuGaS2 single crystals grown by CVT method and their characterization, J. Phys. D Appl. Phys. 41 (2008) 11510, https://doi.org/10.1088/0022-3727/41/11/115102.

[13] P. Chen, M. Qin, H. Chen, C. Yang, Y. Wang, F. Huang, Cr incorporation in CuGaS2 chalcopyrite: a new intermediate-band photovoltaic material with wide-spectrum solar absorption, Phys. Status Solidi 210 (2013) 1098–1102, https://doi.org/10.1002/pssa.201228721.

[14] S. Kalainathan, N. Ahsan, T. Hoshii, Y. Okada, T. Logu, K. Sethuraman, Tailoring sub-bandgap of CuGaS2 thin film via chromium doping by facile chemical spray pyrolysis technique, J. Mater. Sci. Mater. Electron. 29 (2018) 19359–19367, https://doi.org/10.1007/s10854-018-0065-2.

[15] D. Perednis, L.J. Gauckler, Thin film deposition using spray pyrolysis, J. Electroceram. 14 (2) (2005) 103–111, https://doi.org/10.1007/s10832-005-0870-x.

[16] J.C. Viguie, J. Spitz, Chemical vapor deposition at low temperatures, Polymer. Benzene 122 (4) (1975).

[17] W. Siefert, Corona spray pyrolysis: a new coating technique with an extremely enhanced deposition efficiency, Thin Solid Films 120 (4) (1984) 267–274, https://doi.org/10.1016/0040-6090(84)90241-4.

[18] B. Su, K. Choy, Microstructure and properties of the CdS thin films prepared by electrostatic spray assisted vapour deposition (ESAVD) method, Thin Solid Films 359 (2) (2000) 160–164, https://doi.org/10.1016/S0040-6090(99)00733-6.

[19] X. Hou, K.-L. Choy, Deposition mechanism and structural characterization of TiO2 films produced using ESAVD method, Surf. Coating. Technol. 180–181 (2004) 15–19, https://doi.org/10.1016/j.surfcoat.2003.10.023.

[20] M. Okuya, Porous TiO2 thin films prepared by spray pyrolysis deposition (SPD) technique and their application to UV sensors, Solid State Ionics 172 (1–4) (2004) 527–531, https://doi.org/10.1016/j.ssi.2004.02.060.

[21] J.B. Mooney, S.B. Radding, Spray pyrolysis processing, Annu. Rev. Mater. Sci. 12 (1) (1982) 81–101, https://doi.org/10.1146/annurev.ms.12.080182.000501.

[22] X.-C. He, H.-S. Shen, P. Wu, K. Dwight, A. Wold, Growth and characterization of CuGaS2, CuAlS2 and CuGa0.9Al0.1S2 single crystals, Mater. Res. Bull. 23 (6) (1988) 799–803, https://doi.org/10.1016/0025-5408(88)90072-4.

[23] W.N. Honeyman, Preparation and properties of single crystal CuAlS2 and CuAlSe2, J. Phys. Chem. Solid. 30 (8) (1969) 1935–1940, https://doi.org/10.1016/0022-3697(69)90169-3.

[24] J.L. Shay, P.M. Bridenbaugh, B. Tell, H.M. Kasper, p-type conductivity and green photoluminescence of CuGaS2 grown by iodine transport, J. Lumin. 6 (2) (1973) 140–142, https://doi.org/10.1016/0022-2313(73)90051-3.

[25] C.L. Bailey, L. Liborio, G. Mallia, S. Tomić, N.M. Harrison, Defect physics ofCuGaS2, Phys. Rev. B 81 (20) (2010), https://doi.org/10.1103/physrevb.81.205214.

[26] O. Madelung, U. Rössler, M. Schulz (Eds.), Ternary Compounds, Organic Semiconductors, 41E, Springer-Verlag, 2000, https://doi.org/10.1007/b72741.

[27] A.R. Zanatta, Revisiting the optical bandgap of semiconductors and the proposal of a unified methodology to its determination, Sci. Rep. 9 (1) (2019) 11225, https://doi.org/10.1038/s41598-019-47670-y.

[28] J.L. Shay, J.H. Wernick, in: B.R. Pamplin (Ed.), Ternary Chalcopyrite Semiconductors: Growth, Electronic Properties, and Applications, International Series of Monographs in the Science of the Solid State, 1975.

[29] A.D. DeAngelis, K. Horsley, N. Gaillard, Wide band gap CuGa(S,Se) 2 thin films on transparent conductive fluorinated tin oxide substrates as photocathode candidates for tandem water splitting devices, J. Phys. Chem. C 122 (26) (2018) 14304–14312, https://doi.org/10.1021/acs.jpcc.8b02915.

[30] J.A. Hollingsworth, W.E. Buhro, A.F. Hepp, P.P. Jenkins, M.A. Stan, Spray chemical vapor deposition of CuInS 2 thin films for application in solar cell devices, MRS Proc. 495 (1997) 171, https://doi.org/10.1557/PROC-495-171.

[31] W.-J. Jeong, G.-C. Park, Structural and electrical properties of CuGaS2 thin films by electron beam evaporation, Sol. Energy Mater. Sol. Cell. 75 (1–2) (2003) 93–100, https://doi.org/10.1016/S0927-0248(02)00110-1.

[32] N. Ahsan, S. Kalainathan, N. Miyashita, T. Hoshii, Y. Okada, Characterization of Cr Doped CuGaS2 Thin Films Synthesized by Chemical Spray Pyrolysis, Mechanics, Materials Science & Engineering, 2017.

[33] L. Wang, X. Yuan, Y. Wang, W. Yao, J. Zhu, W. Jing, Preparation and characterization of CuGaS2 thin films as a promising parent material for intermediate band solar cells, Mater. Sci. Semicond. Process. 30 (2015) 267–270, https://doi.org/10.1016/j.mssp.2014.10.007.

[34] P. Prabukanthan, R. Dhanasekaran, Growth of CuGaS2 single crystals by chemical vapor transport and characterization, Cryst. Growth Des. 7 (4) (2007) 618–623, https://doi.org/10.1021/cg060450o.

[35] M.A.S. Andrade, L.H. Mascara, Bismuth doping on CuGaS2 thin films: structural and optical properties, MRS Commun. 8 (2) (2018) 504–508, https://doi.org/10.1557/mrc.2018.63.

[36] M.M. Han, X.L. Zhang, Z. Zeng, Sn doping induced intermediate band in CuGaS2, RSC Adv. 6 (112) (2016) 110511–110516, https://doi.org/10.1039/C6RA16855H.

[37] K. Sankarasubramanian, P. Soundarrajan, T. Logu, S. Kiruthika, K. Sethuraman, R. Ramesh Babu, K. Ramamurthi, Influence of Mn doping on structural, optical and electrical properties of CdO thin films prepared by cost effective spray pyrolysis method, Mater. Sci. Semicond. Process. 26 (2014) 346–353, https://doi.org/10.1016/j.mssp.2014.05.005.

[38] F. Belarbi, M. Adnane, F. Boutaiba, Structural and Electronic Properties for Chalcopyrite Semiconducting Materials Based on CuXS2 (X = In, Ga and Al): AB-Initio Computational Study, 2020, pp. 375–381, https://doi.org/10.1007/978-981-15-5444-5_47.

[39] L. Jorge, Cholula-Díaz, Jose Barzola-Quiquia, Christian Kranert, Tom Michalsky, Pablo Esquinazi, Marius Grundmann, Harald Krautscheid, Conducting behavior of chalcopyrite-type CuGaS2 crystals under visible light, Phys. Chem. Chem. Phys. (2010) 1–7.

[40] Kenneth Barbalace (n.d.). Environmental, Chemistry & Hazardous Materials News, Careers & Resources. Ionic Radius..

[41] U. Caudillo-Flores, A. Kubacka, T. Berestok, T. Zhang, J. Llorca, J. Arbiol, A. Cabot, M. Fernández-García, Hydrogen photogeneration using ternary CuGaS2-TiO2-Pt nanocomposites, Int. J. Hydrogen Energy 45 (3) (2020) 1510–1520, https://doi.org/10.1016/j.ijhydene.2019.11.019.

[42] S.-H. Chang, B.-C. Chiu, T.-L. Gao, S.-L. Jheng, H.-Y. Tuan, Selective synthesis of copper gallium sulfide (CuGaS2) nanostructures of different sizes, crystal phases, and morphologies, CrystEngComm 16 (16) (2014) 3323–3330, https://doi.org/10.1039/C3CE42530D.

[43] B. Du, R. Zhang, K. Chen, A. Mahajan, M.J. Reece, The impact of lone-pair electrons on the lattice thermal conductivity of the thermoelectric compound CuSbS 2, J. Mater. Chem. A 5 (7) (2017) 3249–3259, https://doi.org/10.1039/C6TA10420G.

[44] X. Lv, S. Yang, M. Li, H. Li, J. Yi, M. Wang, G. Niu, J. Zhong, Investigation of a novel intermediate band photovoltaic material with wide spectrum solar absorption based on Ti-substituted CuGaS2, Sol. Energy 103 (2014) 480–487, https://doi.org/10.1016/j.solener.2014.02.046.

[45] Q. Li, C. Zou, L. Zhai, J. Shen, L. Zhang, H. Yu, Y. Yang, X. Chen, S. Huang, Growth of wurtzite CuGaS2 nanoribbons and their photoelectrical properties, J. Alloys Compd. 567 (2013) 127–133, https://doi.org/10.1016/j.jallcom.2013.03.023.
[46] M.G. Goydaragh, A.A. Jafarzadeh, F. Shahbazi, S. Oustan, R. Taghizadeh-Mehrjardi, M. Lado, Estimation of elemental composition of agricultural soils from West Azerbaijan, Iran, using mid-infrared spectral models, Rev. Bras. Eng. Agrícola Ambient. 23 (6) (2019) 460–466, https://doi.org/10.1590/1807-1929/agriambi.v23n6p460-466.
[47] J.P. Tailor, S.H. Chaki, M.P. Deshpande, Comparative study between pure and manganese doped copper sulphide (CuS) nanoparticles, Nano Express 2 (1) (2021) 010011, https://doi.org/10.1088/2632-959X/abdc0d.
[48] T. Maeda, W. Gong, T. Wada, Crystallographic and optical properties and band structures of CuInSe 2 , CuIn 3 Se 5 , and CuIn 5 Se 8 phases in Cu-poor Cu 2 Se–In 2 Se 3 pseudo-binary system, Jpn. J. Appl. Phys. 55 (4S) (2016) 04ES15, https://doi.org/10.7567/JJAP.55.04ES15.
[49] S.N. Malik, A.Q. Malik, R.F. Mehmood, G. Murtaza, Y.G. Alghamdi, M.A. Malik, AACVD of Cu 2−x S, In 2 S 3 and CuInS 2 thin films from [Cu(i Bu 2 PS 2)(PPh 3) 2] and [In(i Bu 2 PS 2) 3] as single source precursors, New J. Chem. 39 (5) (2015) 4047–4054, https://doi.org/10.1039/C4NJ02289K.
[50] Y. Zhang, J.Y. Park, S.Y. Park, S.O. Ryu, S.O. Ryu, Study on the CIGS thin film formation by modified spray process, Mol. Cryst. Liq. Cryst. 602 (1) (2014) 234–243, https://doi.org/10.1080/15421406.2014.944781.
[51] E. Aydin, M. Sankir, N.D. Sankir, Conventional and rapid thermal annealing of spray pyrolyzed copper indium gallium sulfide thin films, J. Alloys Compd. 615 (2014) 461–468, https://doi.org/10.1016/j.jallcom.2014.06.140.
[52] A.S. Hassanien, A.A. Akl, Effect of Se addition on optical and electrical properties of chalcogenide CdSSe thin films, Superlattice. Microst. 89 (2016) 153–169, https://doi.org/10.1016/j.spmi.2015.10.044.
[53] M. Isik, H.H. Gullu, E. Coskun, N.M. Gasanly, Optical band gap and dispersion of optical constants of Cu-Ga-S thin films, Optik 186 (2019) 147–154, https://doi.org/10.1016/j.ijleo.2019.04.035.
[54] S. Gahlawat, J. Singh, A.K. Yadav, P. Ingole, Exploring Burstein-Moss type effect in nickel doped hematite dendrite nanostructure for enhanced photo-electrochemical water splitting, Phys. Chem. Chem. Phys. (2019), https://doi.org/10.1039/c9cp04132j.
[55] P. Makuła, M. Pacia, W. Macyk, How to correctly determine the band gap energy of modified semiconductor photocatalysts based on UV–vis spectra, J. Phys. Chem. Lett. 9 (23) (2018) 6814–6817, https://doi.org/10.1021/acs.jpclett.8b02892.
[56] Hadri Adil, Abderrahim El Hat, Mouaad Sekkati, Mzerd Ahmed, Investigation of Structural, Optical, and Electrical Properties of In-Doped SnO2 Thin Films Deposited by Spray Pyrolysis, vols. 1–4, 2017.
[57] B.M. Başol, in: L.A. Eldada (Ed.), Application of Electrochemical Deposition Techniques to Thin Film Solar Cell Processing, 2011, https://doi.org/10.1117/12.896362, 81100Q.
[58] R. Kaigawa, A. Neisser, R. Klenk, M.-C. Lux-Steiner, Improved performance of thin film solar cells based on Cu(In,Ga)S2, Thin Solid Films 415 (1–2) (2002) 266–271, https://doi.org/10.1016/S0040-6090(02)00554-0.